

# Guided Multi-objective Generative AI to Enhance Structure-based Drug Design

Amit Kadan <sup>\*a‡</sup>, Kevin Ryczko <sup>\*a‡</sup>, Erika Lloyd<sup>a</sup>, Adrian Roitberg<sup>b</sup>, Takeshi Yamazaki<sup>\*a</sup>

Generative AI has the potential to revolutionize drug discovery. Yet, despite recent advances in deep learning, existing models cannot generate molecules that satisfy all desired physicochemical properties. Herein, we describe IDOLpro, a novel generative chemistry AI combining diffusion with multi-objective optimization for structure-based drug design. Differentiable scoring functions guide the latent variables of the diffusion model to explore uncharted chemical space and generate novel ligands *in silico*, optimizing a plurality of target physicochemical properties. We demonstrate our platform’s effectiveness by generating ligands with optimized binding affinity and synthetic accessibility on two benchmark sets. IDOLpro produces ligands with binding affinities over 10%-20% higher than the next best state-of-the-art method on each test set, producing more drug-like molecules with generally better synthetic accessibility scores than other methods. We do a head-to-head comparison of IDOLpro against a classic virtual screen of a large database of drug-like molecules. We show that IDOLpro can generate molecules for a range of important disease-related targets with better binding affinity and synthetic accessibility than any molecule found in the virtual screen while being over 100× faster and less expensive to run. On a test set of experimental complexes, IDOLpro is the first to produce molecules with better binding affinities than the experimentally observed ligands. IDOLpro can accommodate other scoring functions (e.g. ADME-Tox) to accelerate hit-finding, hit-to-lead, and lead optimization for drug discovery.

## 1 Introduction

The central goal of structure-based drug design (SBDD) is to design ligands with high binding affinities given a 3-dimensional protein pocket<sup>1</sup>. SBDD is inherently an inverse design problem, where the desired properties (high binding affinity to a target protein, synthesizability etc.) are known, but the design of a molecule with the desired properties is non-trivial. Inverse design problems are prevalent in the materials<sup>2-4</sup>, chemical<sup>5-7</sup>, and life sciences<sup>8-10</sup>. They have two fundamental steps: The sampling of a chemical space, and the scoring (or evaluation) of compounds’ ability to satisfy the set of desired properties. The sampling of chemical space can be done in various ways. For drug discovery, the typical way to achieve this is by evaluating each entry of a large database of drug-like molecules such as ZINC<sup>11</sup>, Enamine<sup>12</sup>, or GDB<sup>13</sup>, collect the results and rank them accordingly to yield a shortlist of compounds to be screened in a laboratory. Although these databases can contain hundreds of billions of molecules<sup>13</sup>, this is just a fraction of drug-like chemical space which is estimated to number anywhere between  $10^{20} - 10^{60}$  molecules<sup>14</sup>.

In the recent literature, a flurry of generative deep learning

(DL) models have been proposed to replace the virtual screening of large databases<sup>15-20</sup>. In Ref.<sup>16</sup>, an equivariant probabilistic model called Pocket2Mol was trained to sequentially generate new atoms in a protein given the current atomic context. In Ref.<sup>18</sup>, an equivariant diffusion model called TargetDiff was introduced to generate ligands from scratch. They also showed that their model can be used as an unsupervised predictor of binding affinity. In Ref.<sup>19</sup>, two other equivariant diffusion models were introduced to generate a ligand from scratch. These models are also able to perform scaffold-hopping and fragment merging/growing, both of which are facilitated by an inpainting-inspired<sup>21</sup> molecular generation scheme. In all three references, the ligands produced by the models attained lower average Vina scores<sup>22</sup> than docked molecules in the test set. Sampling ligands by using these models is not only more efficient than searching through a database, but they are also capable of producing new molecules that don’t currently exist in molecular databases<sup>20</sup>, expanding the chemical space available during the drug-discovery process. However, in some cases they have been shown to produce ligands that do not exhibit desired physicochemical properties such as unphysical structures (aromatic rings which are not flat, overly small or large bond lengths etc.)<sup>23,24</sup>, or synthesizability<sup>25</sup>. To work in an inverse design pipeline, these models must be paired with an evaluation scheme to filter and rank molecules based on required attributes. Additionally, a feedback loop from the evaluation scheme to the generator can be introduced, allowing one to condition generation on measured physicochemical indicators, and improving

<sup>a</sup> SandboxAQ, Palo Alto, CA, United States

<sup>b</sup> Department of Chemistry, University of Florida, PO Box 117200, Gainesville, 2611-7200, Florida, United States.

\* Corresponding Authors: amit.kadan@sandboxaq.com, kevin.ryczko@sandboxaq.com, takeshi.yamazaki@sandboxaq.com

‡ Equal Contributions: amit.kadan@sandboxaq.com, kevin.ryczko@sandboxaq.com

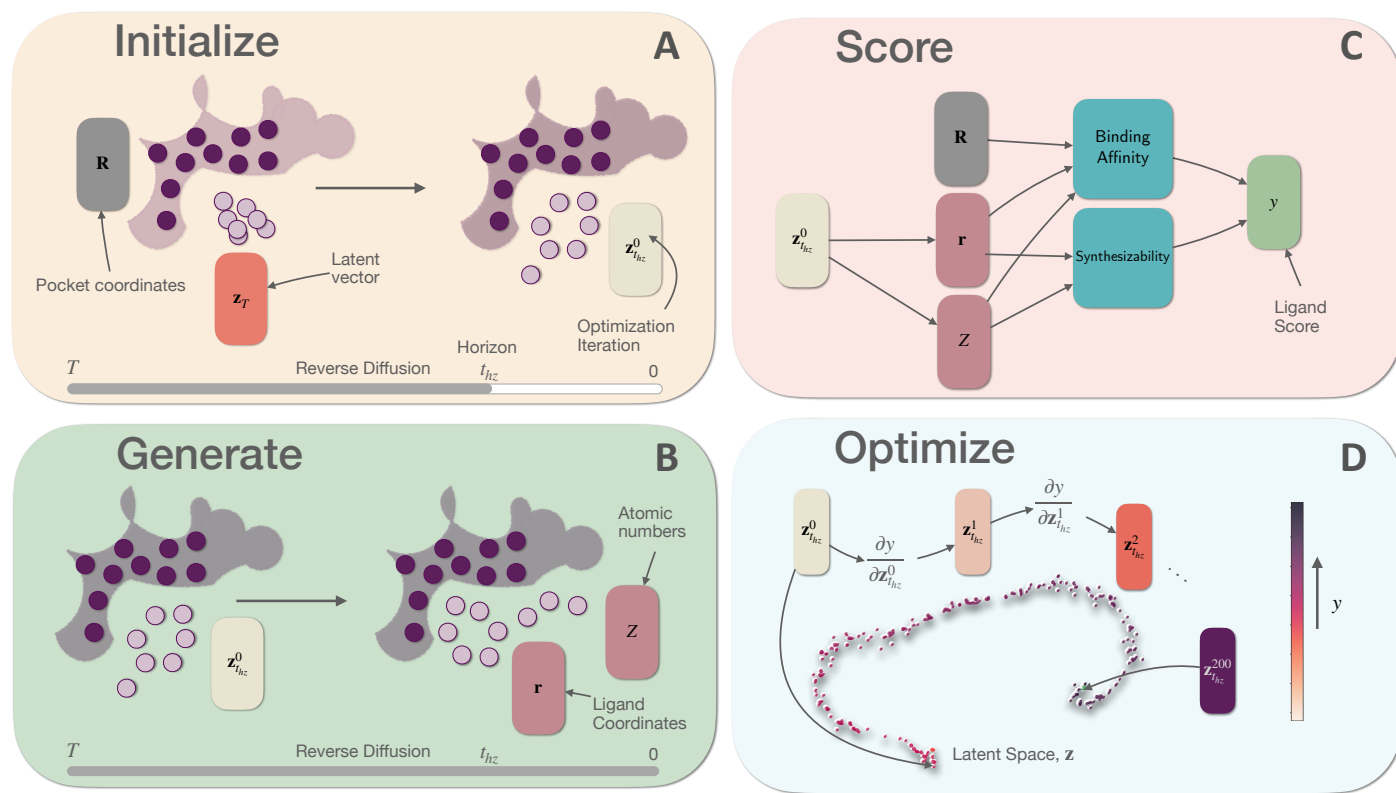


Fig. 1 Visual overview. A: Random latent vectors are defined (this is skipped when seeded with a known ligand) and the reverse diffusion is run for  $T \rightarrow t_{hz}$ . B: The rest of the reverse diffusion process is completed and a ligand is generated (with coordinates and atomic numbers). C: The ligand is scored by evaluating the binding affinity, synthesizability, or both. D: The ligand score is differentiated with respect to the latent vector  $z_{hz}^0$ , and  $z_{hz}^1$  is defined by taking a single optimization step.

the sampling of chemical space to yield molecules with better target properties. This feedback loop is essential to accelerate the design process given the size of chemical space<sup>6,8,26</sup>.

Conditional generation is becoming a common practice in the drug-discovery literature. Ref.<sup>20</sup> pairs a policy network with a Monte Carlo Tree Search algorithm to design ligands with optimized Vina scores. They apply their methodology to the inhibitor design for the main protease of SARS-CoV-2, producing novel ligands with high binding affinity. Similarly, Ref.<sup>19</sup> pairs a diffusion model with an evolutionary algorithm to optimize the properties of the generated ligands given an initial ligand. Ref.<sup>27</sup> uses property predictors to guide a generative model composed of an equivariant autoencoder and transformer decoder in generating molecules with high target properties. A disadvantage of these works is that they do not use gradient information for the objectives in their optimization schemes, making them scale worse with the degrees of freedom of the problem<sup>28</sup>.

In this work, we present IDOLpro (Inverse Design of Optimal Ligands for Protein pockets) that can produce an optimized set of chemically feasible ligands given a protein pocket. IDOLpro guides state-of-the-art diffusion models to produce optimized ligands for a given protein pocket. Specifically, we modify the latent variables of the generative model to optimize one or more objectives of interest simultaneously. The objectives considered evaluate properties of the generated ligands and in this report, we include binding affi-

ity and synthetic accessibility. Although we only explore a single diffusion model for generation, and these two metrics for scoring, our framework is highly modular and can easily incorporate alternative generators and additional scores. To estimate binding affinity, we have integrated several objectives, including a torch-based version of Vina<sup>22</sup> that we call torchvina, DiffDock score<sup>29</sup>, and the ANI2x model<sup>30</sup>. To estimate synthetic accessibility, we train an equivariant neural network model to predict the SA score reported from RDKit<sup>31</sup>. All metrics are written in PyTorch<sup>32</sup> and are fully differentiable with respect to the latent variables within the diffusion model, allowing for the use of gradient-based optimization strategies to design optimal ligands.

In two recent works, gradients from property predictors were used to guide a diffusion model in generating molecules with optimized properties<sup>8,10</sup>. These works require a property predictor capable of making predictions on noisy, intermediate representations of molecules to guide diffusion at each step. An advantage of these related works is that once this auxiliary property predictor is produced, reverse diffusion only has to be run once for each generated molecule. IDOLpro requires re-running reverse diffusion multiple times, resulting in additional computational costs. However, a major advantage of our platform is that it can incorporate any differentiable score capable of making predictions on molecular structures, allowing for the integration of novel metrics without needing to develop models from scratch.

## 2 Results

### 2.1 Workflow

IDOLpro takes the protein pocket information as input and iteratively modifies the predictions of a generator that generates molecules directly into the pocket to produce optimal ligands according to a set of differentiable scores defining target properties. IDOLpro accomplishes this task by modifying the latent vectors of the generative model with gradients from the property predictors. Once a set of optimal ligands are produced, their binding poses are further refined by performing structural optimization within the pocket. The structural optimization algorithm interfaces with the same differentiable scores used for latent optimization and iteratively modifies the ligands’ coordinates with gradients from the property predictors. A visual overview of IDOLpro is pictured in Fig. 1.

In this report, our method uses DiffSBDD<sup>19</sup> as the baseline generative method for predicting ligands within a protein pocket. We use a specific variant of the model, DiffSBDD-Cond, which we found was able to generate ligands within the protein pocket without clashes more reliably than the alternative, DiffSBDD-inpaint. We assess the ability of our framework to discover novel ligands with improved binding affinity and synthetic accessibility. To evaluate and be able to gather gradient information for binding affinity, we have developed a torch-based implementation of the Vina score<sup>22</sup>, which we refer to as torchvina. To evaluate synthetic accessibility, we have trained an equivariant neural network model to predict the synthetic accessibility (SA) score first proposed in Ref.<sup>33</sup>, which we refer to as torchSA.

### 2.2 Datasets

We assess the performance of IDOLpro on three different test sets – a subset of CrossDocked<sup>34</sup>, a subset of the Binding MOAD (Mother of all Databases)<sup>35</sup>, and on a test set consisting of disease-related proteins first proposed in Ref.<sup>36</sup>, which we refer to as the RGA test set.

All three databases contain protein pocket-ligand pairs. The CrossDocked dataset contains 100 pocket-ligand pairs which were derived via re-docking ligands to non-cognate receptors with smina<sup>37</sup>. This test set was used to validate the performance of tools in several other papers<sup>15,16</sup>, including DiffSBDD<sup>19</sup>. The Binding MOAD contains 130 high-resolution (<2.5 Å) experimentally derived pocket-ligand pairs extracted from the Protein Data Bank (PDB). This test set was also used to assess the performance of DiffSBDD. The RGA test set consists of 10 disease-related protein targets including G-protein coupling receptors (GPCRs) and kinases from the DUD-E dataset<sup>38</sup>, as well as the SARS-CoV-2 main protease<sup>39</sup>. This is also an experimentally derived test set and was used to assess the performance of several non-deep learning-based methods in Ref<sup>36</sup>.

### 2.3 Validation of Latent Vector Optimization

To assess the ability of IDOLpro to augment the performance of the baseline model via the optimization of latent vectors, we run IDOLpro to optimize torchvina and torchSA, and analyze its capability

to improve the Vina and SA scores relative to DiffSBDD-Cond. For each of the protein pockets in the CrossDocked and Binding MOAD test sets, we generate 100 optimized ligands using IDOLpro. We calculate the Vina and SA scores of ligands before and after latent vector optimization with IDOLpro. We report the average Vina and SA scores, and the top-10% Vina and SA scores for each method on each test set. We also report the average percentage of synthesizable molecules generated. In this work, we define a ligand as synthesizable if it achieves an SA score of less than 3.5. Although the inventors of the SA score suggest 6 as the cutoff for synthesizability, a number of papers have found SA scores between 3.5 and 6 to be ambiguous<sup>25,40</sup>. A cutoff of 3.5 was also used to determine synthesizability in Ref.<sup>41</sup>.

The results are shown in Table 1. We find that IDOLpro generates ligands with better Vina and SA scores than DiffSBDD-cond, yielding molecules with  $\approx 20\%$  better Vina scores and  $\approx 21\%$  better SA scores on the CrossDocked dataset, and  $\approx 26\%$  better Vina scores and  $\approx 21\%$  better SA scores on the Binding MOAD dataset. Furthermore, IDOLpro yields more than double the amount of synthesizable ligands compared with DiffSBDD-cond for each dataset (51.2 % vs 23.5 % and 56.9 % vs 22.6 %). Overall, IDOLpro is able to co-optimize Vina and SA, producing molecules with significantly better binding affinities and synthetic accessibility when compared to the baseline model, DiffSBDD-cond.

### 2.4 Comparison to Deep Learning

We compare our full pipeline, including both latent vector optimization and structural refinement, to other deep learning tools in the literature on the CrossDocked and Binding MOAD test sets. As was done in Ref<sup>19</sup>, for each protein pocket, we generate 100 optimized ligands using IDOLpro. Aside from reporting the Vina score, top-10% Vina score, and SA score, we report several other metrics widely reported in the literature. We evaluate the QED (quantitative estimate of drug-likeness)<sup>44</sup>, a metric combining several desirable molecular properties for screening drug-like molecules. We report diversity – the average pairwise dissimilarity between all generated molecules for a given protein pocket. Dissimilarity is measured as  $1 - \text{Tanimoto similarity}$ . Lastly, we report the average time taken to generate a single ligand with each framework. These metrics are evaluated across six other DL tools in the literature: 3D-SBDD<sup>15</sup>, Pocket2Mol<sup>16</sup>, GraphBP<sup>17</sup>, TargetDiff<sup>18</sup>, DiffSBDD-Cond, and DiffSBDD-inpaint<sup>19</sup>. Results for other tools are taken from Ref.<sup>19</sup>. IDOLpro is run to completion from start to finish, first optimizing latent vectors, followed by structural refinement. Other tools have their ligands docked with QuickVina2<sup>45</sup> after generation as was done in Ref.<sup>19</sup>. Full results are shown in Table 2. The performance of the models on the two optimized metrics – Vina and SA is visualized in Fig. 2. Examples of molecules produced by IDOLpro are shown in Fig. 3.

For CrossDocked, IDOLpro achieves greatly improved Vina scores relative to other DL tools, with a 0.71 kcal/mol improvement in average Vina score and 1.03 kcal/mol improvement in top-10% Vina score compared to the next best tool in the literature, DiffSBDD-inpaint. Despite not optimizing QED directly, we

Dataset	Method	Vina [kcal/mol]	Vina <sub>10%</sub> [kcal/mol]	SA	SA <sub>10%</sub>	Synth [%]
CrossDocked	DiffSBDD-cond <sup>19</sup>	-5.37 ± 1.93	-7.70 ± 2.25	4.30 ± 0.50	2.56 ± 0.63	23.5 ± 15.5
	IDOLpro	-6.47 ± 2.10	-8.69 ± 2.45	3.41 ± 0.70	1.73 ± 0.51	51.2 ± 22.7
MOAD	DiffSBDD-cond <sup>19</sup>	-5.38 ± 2.55	-7.66 ± 2.37	4.18 ± 0.50	2.50 ± 0.53	26.5 ± 17.8
	IDOLpro	-6.77 ± 2.24	-8.68 ± 2.56	3.32 ± 0.66	1.79 ± 0.46	56.9 ± 22.6

Table 1 Performance of IDOLpro when used to optimize torchvina and torchSA relative to the baseline model, DiffSBDD-cond on the CrossDocked and Binding MOAD test sets. The average Vina score, top-10% Vina score, SA score, top-10% SA score, and the average percent of synthesizable molecules are reported.

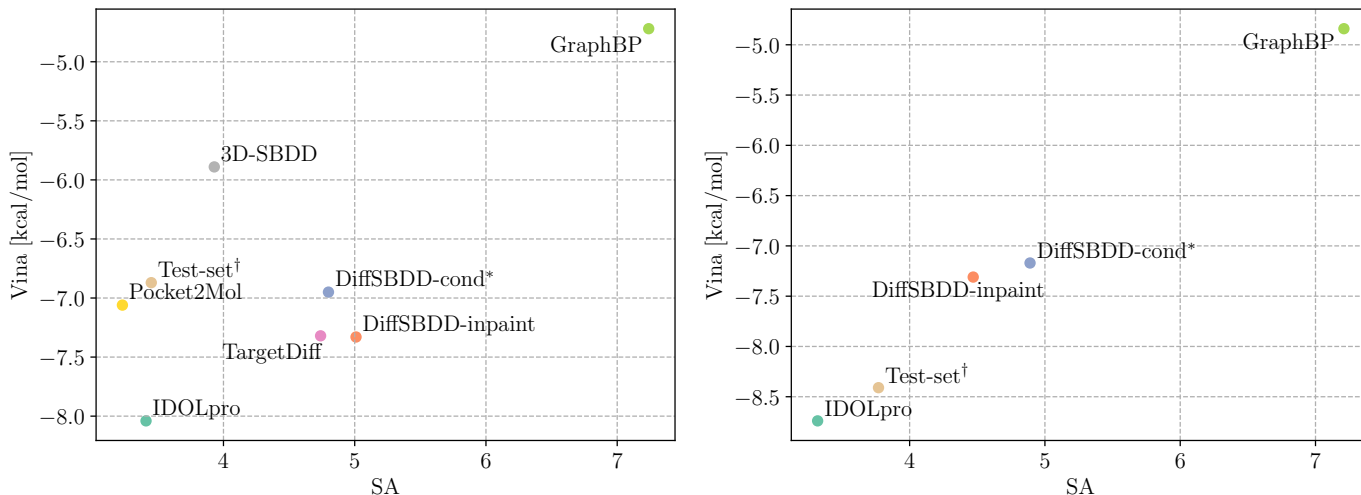


Fig. 2 Performance of DL tools on two benchmark test sets. The scatter plot shows the average Vina and SA score for each method for targets in CrossDocked (left), and the Binding MOAD (right). IDOLpro is at the bottom left of each scatter plot, showing it can co-optimize Vina and SA for generated ligands.

† Vina scores of reference ligands in the test set, redocked with QVina.

\* Baseline method for IDOLpro.

	Method	Vina [kcal/mol]	Vina <sub>10%</sub> [kcal/mol]	SA	QED	Diversity	Time [s/ligand]
CrossDocked	Test Set	-6.87 ± 2.32	-	3.45 ± 1.26	0.48 ± 0.20	-	-
	3D-SBDD <sup>15</sup>	-5.89 ± 1.91	-7.29 ± 2.34	3.93 ± 1.26	0.50 ± 0.17	0.74 ± 0.09	328.13 ± 245.43
	Pocket2Mol <sup>16</sup>	-7.06 ± 2.80	-8.71 ± 3.18	<b>3.23 ± 1.08</b>	0.57 ± 0.16	0.74 ± 0.15	41.79 ± 36.84
	GraphBP <sup>17</sup>	-4.72 ± 4.03	-7.17 ± 1.40	7.24 ± 0.81	0.50 ± 0.12	<b>0.84 ± 0.01</b>	<b>0.17 ± 0.02</b>
	TargetDiff <sup>18</sup>	-7.32 ± 2.47	-9.67 ± 2.55	4.74 ± 1.17	0.48 ± 0.20	0.72 ± 0.09	~ 57.22
	DiffSBDD-cond <sup>19</sup>	-6.95 ± 2.06	-9.12 ± 2.16	4.80 ± 1.17	0.47 ± 0.21	0.73 ± 0.07	2.27 ± 0.86
	DiffSBDD-inpaint <sup>19</sup>	-7.33 ± 2.56	-9.93 ± 2.59	5.01 ± 1.08	0.47 ± 0.18	0.76 ± 0.05	2.67 ± 1.22
	IDOLpro	<b>-8.04 ± 2.55</b>	<b>-10.96 ± 3.02</b>	3.41 ± 0.70	<b>0.63 ± 0.06</b>	0.79 ± 0.07	58.80 ± 32.97
MOAD	Test Set	-8.41 ± 2.03	-	3.77 ± 1.08	0.52 ± 0.17	-	-
	GraphBP <sup>17</sup>	-4.84 ± 2.24	-6.63 ± 0.95	7.21 ± 0.81	0.51 ± 0.11	<b>0.83 ± 0.01</b>	<b>0.23 ± 0.03</b>
	DiffSBDD-cond <sup>19</sup>	-7.17 ± 1.89	-9.18 ± 2.23	4.89 ± 1.08	0.44 ± 0.20	0.71 ± 0.08	5.61 ± 1.42
	DiffSBDD-inpaint <sup>19</sup>	-7.31 ± 4.03	-9.84 ± 2.18	4.47 ± 1.08	0.54 ± 0.21	0.74 ± 0.05	6.17 ± 2.08
	IDOLpro	<b>-8.74 ± 2.59</b>	<b>-11.23 ± 3.12</b>	<b>3.32 ± 0.66</b>	<b>0.63 ± 0.08</b>	0.77 ± 0.07	82.30 ± 45.07

Table 2 Evaluation of DL tools on targets from the CrossDocked and Binding MOAD datasets. The average, along with the standard deviation of each metric across the protein pockets in each dataset is reported. The top performing model on each metric is bolded in the corresponding column. Numbers for other models are taken from Ref.<sup>19</sup>. Time is based on running DiffSBDD-cond on our hardware, and adjusting the times reported in Ref.<sup>19</sup> accordingly. IDOLpro and DiffSBDD-Cond were run on an NVIDIA A10G GPU with 24 GB of GPU memory.

find that IDOLpro produces ligands with the best QED out of all DL tools compared. IDOLpro ranks second for producing molecules with good SA scores, showing the ability of the platform to perform multi-objective optimization. Despite needing to run an entire optimization procedure for each ligand, IDOLpro is still computationally tractable, achieving run times competitive with two

other tools – TargetDiff and Pocket2Mol, while achieving a faster runtime than 3D-SBDD.

IDOLpro is almost always able to find ligands that improve upon both the Vina and SA scores relative to the reference ligand, failing to find such a ligand for only one target – the protein pocket defined by ligand x2p bound to the protein with PDB ID 5mma.

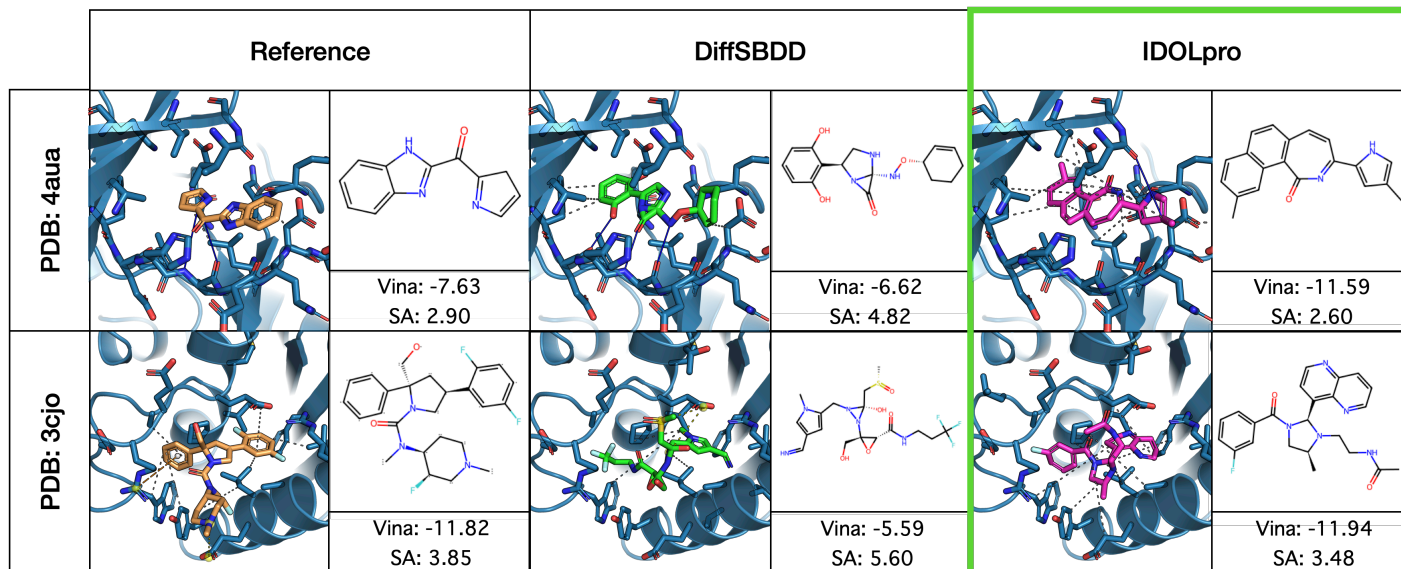


Fig. 3 Molecules produced by IDOLpro when optimizing torchvina and torchSA. One example from each test set is shown – protein 4aua from CrossDocked, and protein 3cjo from the Binding MOAD. Left column: reference molecules from the test sets. Middle column: initial ligand produced by DiffSBDD prior to latent vector optimization. Right column: molecule produced by IDOLpro after optimizing torchvina and torchSA. For each example, the molecule produced by DiffSBDD has worse Vina and SA scores than the reference molecule. After optimization with IDOLpro, both the Vina and SA scores of the generated molecule are better than the reference. Visualizations were created with PyMol<sup>42</sup>, and interactions were visualized with the protein-ligand interaction profiler (PLIP)<sup>43</sup>.

Method	$N_{\text{ligands}}$	Time [h]	Cost [\$]
IDOLpro	$47.20 \pm 49.73$	$0.86 \pm 0.71$	$0.87 \pm 0.72$
Virtual Screen	250,000	$160.90 \pm 24.12$	$109.41 \pm 16.40$

Table 3 Comparison of using IDOLpro to find improved ligands relative to a virtual screen of ZINC250K. We note the average number of ligands, time, and cost it takes for IDOLpro to find a ligand with both better Vina and SA than the best ligand from ZINC250K. Virtual screening was run on an AWS compute-optimized instance with 8 CPU cores, while IDOLpro was run on an NVIDIA A10G GPU with 24 GB of VRAM. Costs are computed based on AWS instance pricing.

For this protein pocket, IDOLpro generated molecules with significantly better SA scores than the reference molecule, but did not generate a single molecule with a better Vina score. We hypothesize that re-weighting the objective in the optimization to more heavily favour the Vina score would allow IDOLpro to generate a ligand that improves upon both metrics.

For the Binding MOAD, the advantage of IDOLpro for generating molecules with high binding affinity is even more pronounced, with a 1.43 kcal/mol improvement in average Vina score, and 1.40 kcal/mol improvement in top-10% Vina score compared to the next best method, DiffSBDD-inpaint. In particular, IDOLpro is the first ML tool to generate molecules with a better average Vina score than those of the reference molecules in the Binding MOAD test set. This is noteworthy, because unlike molecules in CrossDocked, molecules in the Binding MOAD were derived through experiment. Out of the four methods compared, IDOLpro also achieves the best SA, improving upon the next best method by 1.15, while also achieving the best QED despite not optimizing for it directly. The time to generate a single ligand for a protein pocket in the Binding MOAD test set is slower than for the CrossDocked test set, and reflects DiffSBDD’s slowdown in proposing novel molecules for targets in this set.

IDOLpro is able to find a molecule with a better Vina and SA

score than the reference ligand for 126/130 targets ( $\approx 97\%$  of the time). Similar to the one case in CrossDocked for which IDOLpro did not find a ligand with improved Vina and SA score relative to the reference ligand, for these 4 targets IDOLpro finds molecules with significantly better SA scores than the reference, but fails to find a molecule with a better Vina score. All four of these cases have reference molecules with SA scores of over 7, whereas IDOLpro does not produce a single molecule with an SA score over 6. We again hypothesize that this could be solved by re-weighting the optimization objective to more heavily favor Vina score.

Overall IDOLpro can effectively co-optimize multiple objectives, generating ligands with state-of-the-art binding affinity and synthetic accessibility on two test sets. Improving other metrics with IDOLpro is straightforward, simply requiring a differentiable score for evaluating the desired metric. Part of our future work will be to focus on including differentiable scoring functions for other desirable properties such as solubility, toxicity, etc.

## 2.5 Comparison to Virtual Screening

We compare the ability of IDOLpro to generate promising compounds when compared to a virtual screen of a large library of commercially available drug-like compounds. To do so, we evaluate the performance of IDOLpro for finding ligands with high bind-

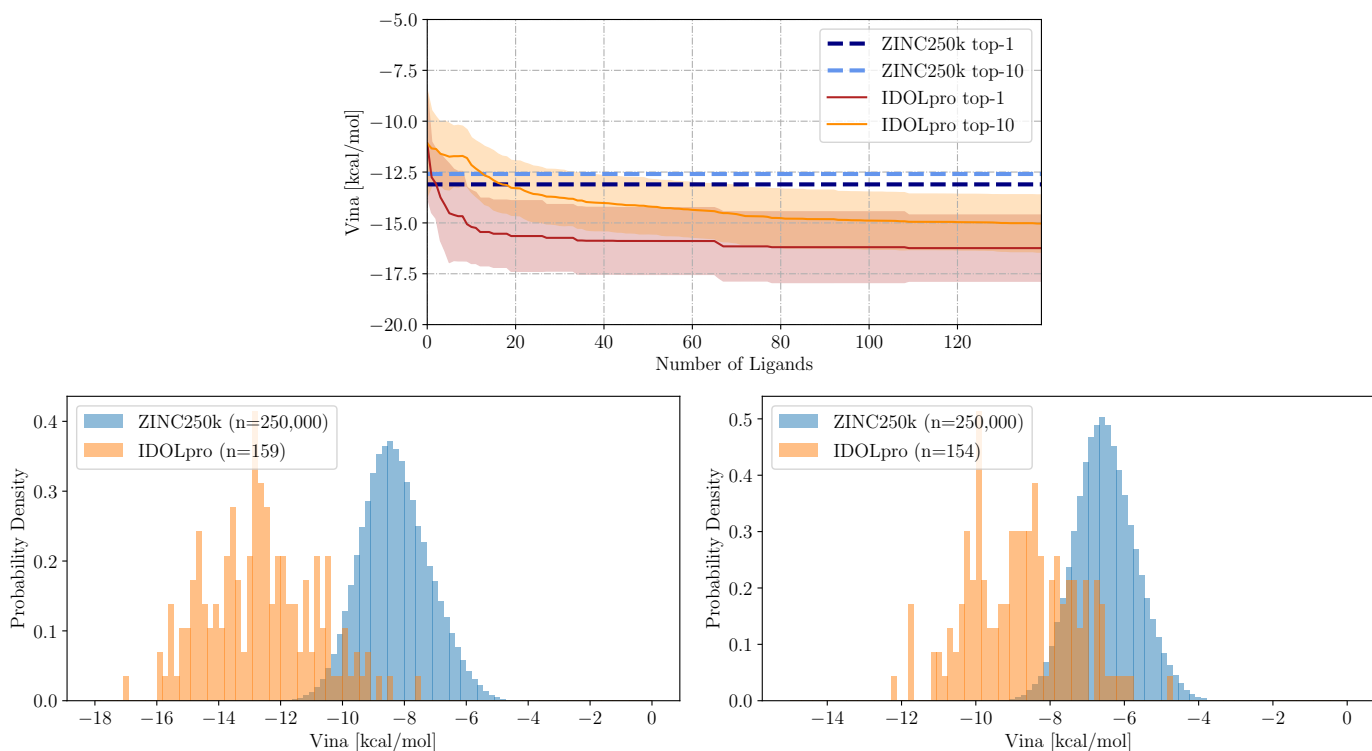


Fig. 4 Comparison of IDOLpro to virtually screening ZINC250K. Top center: The average top-1 and top-10 Vina scores of IDOLpro generated molecules compared to screened molecules from ZINC250K across all 10 targets. Bottom left: The distribution of Vina scores for generated and screened ligands for the SARS-Cov-2 main protease (PDB ID 7l11). Bottom right: The distribution of Vina scores for generated and screened ligands for the EGFR, an important oncology target (PDB ID 2rgp).

Method	Vina <sub>top-100</sub> [kcal/mol]	Vina <sub>top-10</sub> [kcal/mol]	Vina <sub>top-1</sub> [kcal/mol]	SA	QED	Diversity
MARS <sup>46</sup>	-7.76 ± 0.61	-8.8 ± 0.71	-9.26 ± 0.79	2.69 ± 0.08	0.71 ± 0.01	<b>0.88 ± 0.00</b>
MolDQN <sup>47</sup>	-6.29 ± 0.40	-7.04 ± 0.49	-7.50 ± 0.40	5.83 ± 0.18	0.17 ± 0.02	<b>0.88 ± 0.01</b>
GEGL <sup>48</sup>	-9.06 ± 0.92	-9.91 ± 0.99	-10.45 ± 1.04	2.99 ± 0.05	0.64 ± 0.01	0.85 ± 0.00
REINVENT <sup>49</sup>	-10.81 ± 0.44	-11.23 ± 0.63	-12.01 ± 0.83	2.60 ± 0.12	0.45 ± 0.06	0.86 ± 0.01
RationaleRL <sup>50</sup>	-9.23 ± 0.92	-10.83 ± 0.86	-11.64 ± 1.10	2.92 ± 0.13	0.32 ± 0.02	0.72 ± 0.03
GA+D <sup>51</sup>	-8.69 ± 0.45	-9.29 ± 0.58	-9.83 ± 0.32	3.45 ± .12	0.70 ± 0.02	0.87 ± 0.01
Graph-GA <sup>52</sup>	-10.48 ± 0.86	-11.70 ± 0.93	-12.30 ± 1.91	3.50 ± 0.37	0.46 ± 0.07	0.81 ± 0.04
Autogrow 4.0 <sup>53</sup>	-11.37 ± 0.40	-12.21 ± 0.62	-12.47 ± 0.84	2.50 ± 0.05	<b>0.75 ± 0.02</b>	0.85 ± 0.01
RGA <sup>36</sup>	-11.87 ± 0.17	-12.56 ± 0.29	-12.89 ± 0.47	<b>2.47 ± 0.05</b>	0.74 ± 0.04	0.86 ± 0.02
IDOLpro	<b>-14.59 ± 1.51</b>	<b>-16.26 ± 1.66</b>	<b>-17.35 ± 2.10</b>	3.77 ± 0.33	0.64 ± 0.06	0.72 ± 0.04

Table 4 Comparison of IDOLpro to various score and sample-based methods on 10 disease-related protein targets. The average top-100, top-10, and top-1 Vina scores across the targets are reported, along with the average SA, average QED, and diversity. The top-performing model on each metric is bolded in the corresponding column. Numbers for other methods are taken from Ref. <sup>36</sup>.

ing affinity and synthetic accessibility relative to virtually screening the ZINC250K database – a curated collection of commercially available chemical compounds prepared especially for virtual screening containing 250,000 molecules<sup>26</sup>. We evaluate each method on each of 10 protein pockets in the RGA test set.

For this experiment, we measure how quickly IDOLpro can generate a ligand with both better binding affinity (Vina score) and synthetic accessibility (SA score) than the ligand with the best binding affinity found when screening ZINC250K. For screening ZINC250K, we use QuickVina2<sup>45</sup> to quickly dock molecules to each of the 10 target protein pockets in the RGA test set. We run docking on an AWS compute-optimized instance with 8 CPU cores. We

then use IDOLpro to generate optimized ligands, making note of the number of ligands, time, and cost required for IDOLpro to generate an improved ligand relative to virtually screening ZINC250K. Cost is based on the AWS pricing for the requested instances. The results are shown in Table 3.

Screening ZINC250K using QVina takes an average of  $\approx 161$  hours per protein pocket. On the other hand, IDOLpro is able to find a ligand with a better Vina and SA score than the virtual screen in under an hour ( $\approx 52$  minutes) on average. This translates to  $\approx 187\times$  speedup in terms of time, and  $\approx 126\times$  reduction in cost. For 4/10 cases, IDOLpro was able to find a ligand with better Vina and SA score within the first 10 ligands generated, and for

9/10 cases within the first 100 ligands generated. For a single case (PDB ID 3eml) IDOLpro needed to produce 152 ligands to find a ligand with better binding affinity and synthetic accessibility than the one found during the virtual screen. Even in this case, running IDOLpro took  $\approx 2.5$  hours to run on the requested GPU instance, translating to a  $> 60\times$  speedup in terms of time, and  $> 40\times$  reduction in cost compared to virtually screening ZINC250K.

In general, for a given protein pocket, IDOLpro produces ligands with significantly better binding affinities than those found when screening a standard commercially available drug database such as ZINC250K. In Fig. 4, we track the average running top-1 and top-10 Vina scores for IDOLpro across the 10 protein targets as a function of the number of ligands generated. For both the top-1 and top-10 Vina score, IDOLpro quickly surpasses the virtual screen of ZINC250K – needing to generate on average only 3 ligands to surpass the top-1 Vina score of the virtual screen, and needing to generate on average only 13 ligands to surpass the top-10 Vina score of the virtual screen. We also plot the distribution of Vina scores for both the ligands produced by IDOLpro, and those found when screening ZINC250K for 2 of the targets from the RGA test set – 2rgp, a protein whose over-expression has been associated with human tumor growth<sup>54</sup>, and 7111 – the SARS-CoV-2 main protease<sup>39</sup>. These plots are shown in Fig. 4. These plots further validate IDOLpro’s ability to generate ligands with high binding affinity relative to virtual screening.

## 2.6 Comparison to Other Methods

Lastly, we compare IDOLpro to various non-deep learning-based methods in the literature. These methods include genetic algorithms<sup>36,51–53</sup>, reinforcement learning<sup>47–50</sup>, and an MCMC method<sup>46</sup>. We evaluate these methods across the 10 protein pockets in the RGA test set. For each target, as was done in Ref.<sup>36</sup>, we generate 1000 ligands with IDOLpro and calculate the average top-100, top-10, and top-1 Vina score. We also record the average SA and QED of molecules, along with the average diversity per protein pocket. Numbers for other methods are taken from Ref.<sup>36</sup>. Results are shown in Table 4.

IDOLpro greatly outperforms non-DL techniques in terms of Vina score, improving on the next best method by  $\approx 23\%$ ,  $\approx 29\%$ , and  $\approx 35\%$  in terms of average top-100, top-10, and top-1 Vina score respectively. Unlike when compared to other DL methods, IDOLpro ranks behind most of these methods in terms of average SA, ranking 9<sup>th</sup> out of the 10 methods compared. IDOLpro is middle-of-the-pack in terms of QED, ranking 5th out of the 10 methods compared. This shows that IDOLpro, and deep learning methods in general, have a ways to go before they can produce molecules with the same synthesizability and drug-likeness as other advanced non-DL methods in the literature. This is an ongoing area of research<sup>23,25</sup>, and is an aspect that we would like to improve in IDOLpro.

## 2.7 Lead Optimization

In addition to *de novo* generation, IDOLpro can also be used to optimize a known ligand in the protein pocket. This functionality is useful for a common task in drug discovery pipelines known as

lead optimization, where a molecule is progressed from an initial promising candidate towards having optimal properties<sup>55</sup>. Generally, this is accomplished by fixing a large part of the molecule, i.e., the scaffold, while optimizing the rest of the molecule<sup>56</sup>, which is incorporated into the generation with DiffSBDD<sup>19</sup> using an in-painting method.

To perform lead optimization, we specify atoms to fix based on the scaffold of the reference ligand. At each timestep, the fixed atoms are noised, while the rest of the ligand is generated *de novo*. When  $t_{\text{hz}}$  is reached, the optimization procedure begins with a mask applied to the fixed atoms.

To test the capability of our framework, we use the protein pockets from the CrossDocked test set. For each reference ligand, RDKit is used to identify the Bemis-Murcko scaffold<sup>57</sup>. If no scaffold is found (13 cases), if it is identified to be greater than 90% of the full reference ligand (13 cases), or if it contains atoms not supported by the ANI2x model (3 cases), then these targets are removed from the test set. The lead optimization results with IDOLpro for the remaining 71 protein and scaffold pairs are shown in Table 5 where they are compared to the original reference ligands and their corresponding scaffolds. We report the Vina and SA scores of the undocked scaffolds since their atom coordinates are taken directly from the reference ligands as the seed for IDOLpro.

We find that the average Vina scores of the optimized ligands greatly improve upon the seed scaffolds (2.52 kcal/mol), and also exceed the average values of the reference ligands in the test set (1.59 kcal/mol). Although the average SA is higher, both the top-10% SA score and the top-10% Vina are significantly better than the test set, and are more realistic to consider when assessing lead optimization capability. A molecule with both better SA and Vina scores compared to the reference ligands was found for all but one target, where we were able to improve the SA score but not the Vina score. The reference ligand in this case (ligand m6v bound to the protein with PDB ID 4z2g) was relatively large (50 atoms) while the identified scaffold is only 18 atoms. A possible remedy could be to identify a larger scaffold or, as discussed previously, re-weighting the optimization objective to more heavily favor Vina score.

Two examples of generated molecules that retain the original seed scaffold and successfully improve both the Vina and SA scores compared to the reference ligand are shown in Fig. 5. The first is a case where the identified scaffold is a small portion of the reference (ligand with PDB residue ID ily docked into protein 1a2g), and we see a large diversity in the generated molecules. The second is a case where the scaffold is a large component of reference (ligand with PDB residue ID plp docked into protein 2jjg) where we are effectively optimizing functional groups on a fixed scaffold. We believe our results demonstrate the flexibility of atom fixing in IDOLpro, and its utility in performing lead optimization.

## 3 Discussion

We have presented a framework that is designed to produce optimal ligands with desired properties for a given protein pocket. We accomplish this by constructing a computational graph that begins with the latent variables of a diffusion model and ends with the evaluation of metrics important in drug discovery. The latent vari-

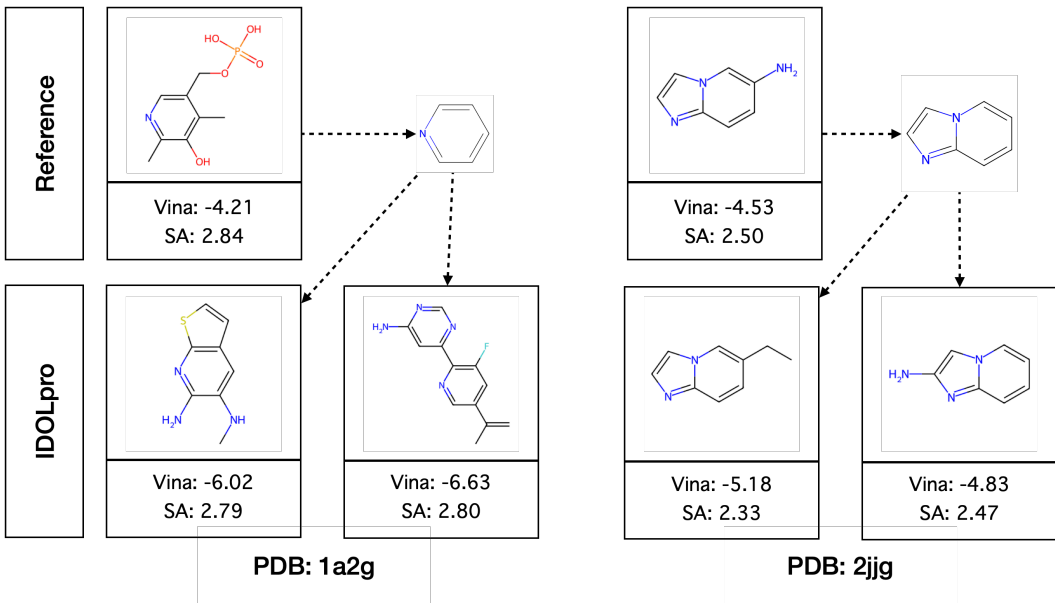


Fig. 5 Molecules produced by IDOLpro during lead optimization. Examples shown are on the ligand 1ly docked into protein 1a2g, and ligand plp docked into protein 2jig, both examples from the CrossDocked test set. IDOLpro is used to append molecules to the scaffold while optimizing torchvina and torchSA. IDOLpro yields multiple ligands with improved SA and Vina relative to the reference molecule.

Method	Vina [kcal/mol]	Vina <sub>10%</sub> [kcal/mol]	SA	SA <sub>10%</sub>
Scaffolds	$-4.65 \pm 2.09$	-	$3.06 \pm 1.40$	-
Test Set	$-5.58 \pm 2.32$	-	$3.67 \pm 1.23$	-
IDOLpro	$-7.17 \pm 2.36$	$-8.96 \pm 2.57$	$4.12 \pm 1.10$	$2.90 \pm 1.12$

Table 5 Results for IDOLPro scaffold fixing on the 71 crossdocked data points with identifiable scaffolds using RDKit’s Bemis-Murcko scaffold. The average and top-10 Vina and SA scores are reported for the seed scaffolds, the reference ligands, and the optimized ligands.

ables can then be modified via standard gradient-based optimization routines to optimize the metrics of interest. More specifically, we perform multivariate optimization by optimizing both Vina and SA scores simultaneously. The molecules generated by our platform achieve the lowest Vina scores when compared to previous, state-of-the-art machine learning methods. When considering the CrossDocked and Binding MOAD test sets, we see a 10% (0.71 kcal/mol) and 20% (1.43 kcal/mol) improvement to the next best tool. Our tool ranks second among all tools compared for producing molecules with good SA scores on CrossDocked, and is state-of-the-art for the Binding MOAD, improving upon the SA of the next best tool by 35%. Furthermore, our tool produces molecules with the highest QED on both datasets. For the Binding MOAD, our framework is the first to produce molecules with a lower average Vina score than reference molecules in the test set, which were derived through experiment. Our tool shows great promise in the hit-finding stage of a standard drug discovery pipeline, finding molecules with better Vina and SA scores at a fraction of the time and cost when compared to a virtual screen of a standard library of commercially available compounds. In addition, our tool can also perform lead optimization by beginning the optimization with a scaffold taken from a reference molecule. When applied to a relevant subset of the CrossDock dataset, we identified ligands with both better SA and Vina scores than the reference ligand in all but one case. Our framework proposes optimal drugs given particular properties, unlocking the ability to virtually screen opti-

mized molecules from a vast chemical space without the need of searching through a vast database, or generating molecules randomly until one with desired properties is found, therefore accelerating the drug discovery process. Our future work will include other important metrics such as toxicity and solubility within the objective to ensure the generation of feasible ligands, along with the consideration of other binding affinity metrics such as free energy perturbation (FEP) based affinity<sup>58</sup>.

## 4 Methods

### 4.1 Generator Module

When optimizing latent vectors, we utilize a state-of-the-art denoising diffusion probabilistic model (DDPM)<sup>59</sup>, DiffSBDD<sup>19</sup>, for generating novel ligands with high binding affinity. DDPMs generate samples from a target distribution by learning the a denoising process. For some  $\tilde{\mathbf{z}}_{data}$  sampled from the target distribution, a diffusion process adds noise to  $\tilde{\mathbf{z}}_{data}$  to elicit the latent vector at time-step  $t$  for  $t = 0, \dots, T$  (where  $T$  is the length of the noising process) according to the transition distributions defined by:

$$p(\mathbf{z}_t | \tilde{\mathbf{z}}_{data}) = \mathcal{N}(\mathbf{z}_t | \alpha_t \tilde{\mathbf{z}}_{data}, \sigma_t^2 \mathbf{I}), \quad (1)$$

$\alpha_t$  controls the level of noise in  $\mathbf{z}_t$  and follows a pre-defined schedule from  $\alpha_0 \approx 1$  (no noise) to  $\alpha_T \approx 0$  (pure noise). In DiffSBDD, the variance-preserving noising process is used, i.e.,  $\alpha_t = \sqrt{1 - \sigma_t^2}$ . The posterior of the transitions conditioned on  $\tilde{\mathbf{z}}_{data}$  define the in-



verse of the noising process, i.e., the denoising process, and can be written in closed form for any  $s < t$ :

$$q(\mathbf{z}_s | \tilde{\mathbf{z}}_{data}, \mathbf{z}_t) = \mathcal{N} \left( \mathbf{z}_s | \frac{\alpha_{t|s} \sigma_s^2}{\sigma_t^2} \mathbf{z}_t + \frac{\alpha_s \sigma_{t|s}^2}{\sigma_t^2} \tilde{\mathbf{z}}_{data}, \frac{\sigma_{t|s}^2 \sigma_s^2}{\sigma_t^2} \mathbf{I} \right), \quad (2)$$

where  $\alpha_{t|s} = \frac{\alpha_t}{\alpha_s}$ , and  $\sigma_{t|s} = \sigma_t^2 - \alpha_{t|s}^2 \sigma_s^2$  following the notation of Ref.<sup>60</sup>. This denoising process relies on  $\tilde{\mathbf{z}}_{data}$ , which is not available during inference. Instead, a neural network,  $\psi_\theta$ , is used to make an inference of  $\hat{\mathbf{z}}_{data}$ . Ref.<sup>59</sup> found that optimization is easier when predicting the noise in the signal. One can reparameterize Eq. (1) such that  $\tilde{\mathbf{z}}_{data} = \frac{1}{\alpha_t} \mathbf{z}_t - \frac{\sigma_t}{\alpha_t} \boldsymbol{\varepsilon}$  where  $\boldsymbol{\varepsilon} \sim \mathcal{N}(\mathbf{0}, \mathbf{I})$ , and get the neural network to predict  $\hat{\boldsymbol{\varepsilon}}_\theta(\mathbf{z}_t, t)$ , yielding a prediction  $\hat{\mathbf{z}}_{data}$ . Thus, given  $\mathbf{z}_t$  and using Eq. (2), one can sample  $\mathbf{z}_s$  for any  $s < t$ . In practice, denoising is done in successive time-steps, i.e.,  $s = t - 1$  in Eq. (2).

DiffSBDD is an  $SE(3)$ -equivariant<sup>61</sup> 3D-conditional DDPM which respects translation, rotation, and permutation symmetries. DiffSBDD was trained to create ligands with high binding affinity given a target protein pocket. In DiffSBDD, data samples consist of protein pocket and ligand point clouds, i.e.,  $\mathbf{z} = [\mathbf{z}^\ell, \mathbf{z}^p]$ . Each point cloud consists of atom types and coordinates,  $\mathbf{z} = [\mathbf{r}, \mathbf{h}]$  where  $\mathbf{r} \in \mathbb{R}^{N \times 3}$  is a tensor of atomic coordinates, and  $\mathbf{h} \in \mathbb{R}^{N \times 10}$  is a tensor of atomic probabilities over the atom types which the model can generate. Within the model, each  $\mathbf{z}_t$  is converted to a graph, and processed by an EGNN<sup>62</sup> to produce a prediction  $\hat{\boldsymbol{\varepsilon}}_\theta(\mathbf{z}_t, t)$ . DiffSBDD contains two different models for 3D pocket conditioning – a conditional DDPM that receives a fixed pocket representation as the context in each denoising step, and a model that is trained to approximate the joint distribution of ligand-protein pocket pairs and is combined with a modified sampling procedure, inpainting<sup>21,63</sup>, at inference time to yield conditional samples of ligands given a fixed protein pocket. In this work, we focus only on the conditional DDPM for ligand generation. Our framework requires that generated ligands do not overlap with the target protein pocket, as the ligands are later docked using structural optimization. We found that the conditional DDPM model is the only model consistently capable of generating ligands satisfying this constraint.

For each pocket-conditioning scheme, DiffSBDD contains two versions of the model - one trained on a subset of CrossDocked<sup>34</sup>, and another trained on a subset of the Binding MOAD<sup>35</sup>. For CrossDocked, Ref.<sup>19</sup> used the same train/test splits as in Ref.<sup>15</sup> and Ref.<sup>16</sup>, resulting in 100,000 complexes for training, and 100 protein pockets for testing. For the Binding MOAD, Ref.<sup>19</sup> filtered the database to contain only molecules with atom types compatible with their model, and removed corrupted entries, resulting in 40,344 complexes for training, and 130 protein pockets for testing. In this work we use only version of DiffSBDD trained on CrossDocked as we found we were able to achieve good results on both test sets (CrossDocked and the Binding MOAD) with just this model.

DiffSBDD was shown to achieve state-of-the-art performance on both test sets. In particular, DiffSBDD achieved the best average, and best top-10% Vina score when compared with other state-of-the-art models in the literature – 3D-SBDD<sup>15</sup>, Pocket2Mol<sup>16</sup>, GraphBP<sup>17</sup>, and TargetDiff<sup>18</sup>. We note, that although DiffSBDD is

used as our baseline model in this report, our framework is not limited to the use of this specific model – any other generative model which makes use of latent vectors as intermediate representations during generation can take its place.

## 4.2 Ligand Validity Checks

When generating ligands using DiffSBDD, we perform several chemical and structural checks to ensure that the generated ligand is valid. A number of these checks are done using RDKit<sup>31</sup>. These include verifying that hydrogens can be added to the ligand and assigned a Cartesian coordinate (using the *addCoords* option in *Chem.AddHs*), that the ligand is not fragmented, and that the ligand can be sanitized. All of these except for the valency check can also be done within DiffSBDD<sup>64</sup>.

In addition, we have four more checks to ensure the structural validity of the ligand. These four checks are necessary to be able to run structural refinement with IDOLpro, which makes use of the ANI2x model<sup>30</sup>. Structural refinement is described in the Structural Refinement Section. We first make sure that the ligand contains only atoms compatible with ANI2x. DiffSBDD can generate ligands with four atom types that are incompatible with ANI2x – B, P, Br, and I. We also make sure that the bond lengths in the ligand are correct by referring to covalent radii, and that the ligand does not overlap with the protein pocket. This is done via ASE’s<sup>65</sup> (Atomic Simulation Environment) *NeighborList* class. Lastly, We make sure that the atoms do not have significant overlap within the ligand itself. This is done via pymatgen’s<sup>66</sup> *Molecule* class.

## 4.3 Scoring Module

After generating a set of ligands, we pass them to a scoring module. In this work, we include a custom torch-based Vina score<sup>22</sup> which we refer to as torchvina, an equivariant neural network trained to predict the synthetic accessibility of molecules with 3D information<sup>33</sup> which we refer to as torchSA, the scoring module from DiffDock<sup>29</sup>, and the ANI2x model<sup>30</sup>. These objectives are all written using Pytorch<sup>32</sup> with differentiable operations and hence can be differentiated automatically using autograd.

**torchvina** We re-implement the Vina force field<sup>22</sup> using Pytorch to allow for automatic differentiation with respect to the latent parameters of the generator. Our work is not the first to produce a Pytorch-based version of Vina to facilitate automatic differentiation, a similar implementation was presented by Ref.<sup>67</sup>. Our motivation for implementing a differentiable Vina score is that docking with Vina was shown to outperform state-of-the-art ML models such as DiffDock<sup>29</sup> when stricter chemical and physical validity checks were enforced on docked molecules, or when these procedures were evaluated on a dataset composed of examples distinct from the ML models’ training data<sup>23</sup>.

The Vina force field is composed of a weighted sum of atomic interactions. Steric, hydrophobic, and hydrogen bonding interactions are calculated and weighted according to a nonlinear fit to structural data<sup>22</sup>. The final score is re-weighted by the number of rotatable bonds to account for entropic penalties<sup>68</sup>. The Vina score is composed of a sum of intramolecular and intermolecular

terms, both of which are integrated into our implementation. Although not used in the study, we have added the ability to score molecules with the Vinardo score<sup>69</sup>, a re-weighted version of the Vina score which was shown to outperform the Vina scores for docking and virtual screening on a number of tests.

**torchSA** To have an evaluator model capable of estimating synthesizability, we train an equivariant neural network to predict the synthetic accessibility (SA) score. SA score was first proposed by Ref.<sup>33</sup>, ranges from 1 (easy to make) and 10 (very difficult to make), and shown to be effective for biasing generative pipelines towards synthesizable molecules<sup>25,70</sup>. Moreover, it was used directly in DiffSBDD to measure the performance of the pipeline<sup>19</sup>. To be able to guide latent parameters in DiffSBDD towards generating ligands with high synthesizability required designing a model that can handle the outputs of DiffSBDD in a differentiable manner. In particular, we constructed a machine learning model that can take in atomic point clouds,  $\mathbf{z} = [\mathbf{r}, \mathbf{h}]$ . We accomplish this by constructing a dataset of atomic point clouds of ligands labeled with SA score. To allow for predictions on probability distributions of atom types, we encode atom types as one-hot vectors. For more details, we refer the reader to the SI.

**ANI2x** ANI2x is a neural network ensemble model that is part of the ANI suite of models<sup>71</sup>. The ANI models are trained on quantum chemistry calculations (at the density functional theory level) and they predict the total energy of a target system. The ANI models are trained on millions of organic molecules and are accurate across different domains<sup>30,72-74</sup>. In addition, they have been shown to outperform many common force fields in terms of accuracy<sup>75</sup>. The ANI models make use of atomic environment descriptors, which probe their local environment, as input vectors. An individual ANI model contains multiple neural networks, each specialized for a specific atom type, predicting the energy contributed by atoms of that type in the molecular system. The total energy of the system is obtained by performing a summation over the atomic contributions<sup>72</sup>. The ANI2x model is an ensemble model consisting of 8 individual ANI models. Each sub-model is trained on a different fold of the ANI2x dataset, composed of gas-phase molecules containing seven different atom types – H, C, N, O, F, Cl, and S<sup>30</sup>. These seven atom types cover  $\approx 90\%$  of drug-like molecules, making ANI2x a suitable ML model for usage in our framework.

#### 4.4 Latent Vector Optimization

The main optimization in IDOLpro occurs via the modification of latent vectors used by the generator to generate novel ligands. We do this by repeatedly evaluating generated ligands with an objective composed of a sum of differentiable scores, calculating the gradient of the objective with respect to the latent vectors (facilitated by automatic differentiation with Pytorch<sup>32</sup>), and modifying the latent vectors via a gradient-based optimizer.

When optimizing latent vectors in DiffSBDD, we do not modify the initial latent vectors used by the model. Instead, we define an optimization horizon,  $t_{\text{hz}}$ . First latent vectors are generated

up to the optimization horizon  $\mathbf{z}_T^\ell, \dots, \mathbf{z}_{t_{\text{hz}}}^\ell$ . This latent vector is saved, and the remaining latent vectors,  $\mathbf{z}_{t_{\text{hz}}-1}^\ell, \dots, \mathbf{z}_0^\ell$ , are generated. Upon passing the ligand validity checks (Section 4.2), the gradient of the objective with respect to  $\mathbf{z}_{t_{\text{hz}}}$  is evaluated, and  $\mathbf{z}_{t_{\text{hz}}}$  is modified using a gradient-based optimizer. When re-generating ligands, rather than starting from  $\mathbf{z}_T^\ell$ , only latent vectors preceding the optimization horizon are re-generated, i.e.,  $\mathbf{z}_{t_{\text{hz}}-1}^\ell, \dots, \mathbf{z}_0^\ell$ . Optimization continues until a maximum number of steps,  $N_{\text{max}}$ , have been taken in the latent space. When de-noising  $\mathbf{z}_t^\ell$  during lead optimization, a mask  $\mathbf{m}_\ell \in \{0, 1\}^{N_\ell}$  is used to keep specific atoms fixed during the inpainting procedure. We employ backtracking, early-stopping, and learning-rate decay, all described in the SI. The optimization of a single ligand is provided in Algorithm 1.

**Algorithm 1** Optimization with IDOLpro

---

```

function IDOLPRO( $\bar{\mathbf{z}}^p, N_\ell, \mathbf{m}_\ell = \mathbf{1}, p = \text{de-novo}, \bar{\mathbf{z}}_0^\ell = \text{None}$ )
  Sample  $\mathbf{z}_T^\ell \sim \mathcal{N}(\mathbf{0}_{N_\ell}, \mathbf{I}_{N_\ell})$ 
  for  $t = T, \dots, t_{\text{hz}} + 1$  do
     $\mathbf{z}_{t-1}^\ell \leftarrow \text{DENOISE}(\mathbf{z}_t^\ell, \bar{\mathbf{z}}^p, \mathbf{m}_\ell, p, \bar{\mathbf{z}}_0^\ell)$ 
  end for
  for  $i = 0, \dots, N_{\text{max}}$  do
    for  $t = t_{\text{hz}}, \dots, 1$  do
       $\mathbf{z}_{t-1}^\ell \leftarrow \text{DENOISE}(\mathbf{z}_t^\ell, \bar{\mathbf{z}}^p, \mathbf{m}_\ell, p, \bar{\mathbf{z}}_0^\ell)$ 
    end for
    if VALIDITY( $\mathbf{z}_0^\ell, \bar{\mathbf{z}}^p$ ) then
       $\mathbf{z}_{t_{\text{hz}}}^\ell \leftarrow \text{ADAM}(\mathbf{z}_{t_{\text{hz}}}^\ell, \frac{\partial(\text{Vina}(\mathbf{z}_0^\ell) + \text{SA}(\mathbf{z}_0^\ell))}{\partial \mathbf{z}_{t_{\text{hz}}}^\ell})$ 
    end if
  end for
  for  $t = t_{\text{hz}}, \dots, 1$  do
     $\mathbf{z}_{t-1}^\ell \leftarrow \text{DENOISE}(\mathbf{z}_t^\ell, \bar{\mathbf{z}}^p, \mathbf{m}_\ell, p, \bar{\mathbf{z}}_0^\ell)$ 
  end for
   $\mathbf{z}_0^\ell \leftarrow \text{STRUCTURALREFINEMENT}(\mathbf{z}_0^\ell)$ 
  return  $\mathbf{z}_0^\ell$ 
end function

function VALIDITY( $\mathbf{z}^\ell, \mathbf{z}^p$ )
   $v \leftarrow \text{VALENCECHECK}(\mathbf{z}^\ell)$ 
   $v \leftarrow v$  and CANSANITIZE( $\mathbf{z}^\ell$ )
   $v \leftarrow v$  and CANADDS( $\mathbf{z}^\ell$ )
   $v \leftarrow v$  and FRAGMENTS( $\mathbf{z}^\ell$ ) = 1
   $v \leftarrow v$  and  $h_i^\ell \in \{H, C, N, O, F, Cl, S\}$ 
   $v \leftarrow v$  and CONNECTED( $\mathbf{z}^\ell$ )
   $v \leftarrow v$  and NOOVERLAPINTRA( $\mathbf{z}^\ell$ )
   $v \leftarrow v$  and NOOVERLAPINTER( $\mathbf{z}^\ell, \mathbf{z}^p$ )
  return  $v$ 
end function

function DENOISE( $\mathbf{z}_t^\ell, \bar{\mathbf{z}}^p, \mathbf{m}_\ell, p, \bar{\mathbf{z}}_0^\ell$ )
  if  $p = \text{de-novo}$  then
     $\mathbf{z}_{t-1}^\ell \leftarrow q(\mathbf{z}_{t-1}^\ell | \mathbf{z}_t^\ell, \mathbf{z}^p)$ 
  else
     $\mathbf{z}_{t-1}^\ell \leftarrow q(\mathbf{z}_{t-1}^\ell | \mathbf{z}_t^\ell, \mathbf{z}^p) \cdot \mathbf{m}_\ell + p(\mathbf{z}_{t-1}^\ell | \mathbf{z}_0^\ell, \mathbf{z}^p) \cdot (1 - \mathbf{m}_\ell)$ 
  end if
end function

```

---

In this work, we focus on using two combinations of evaluators: torchvina on its own, and torchvina in combination with torchSA. We use the Adam<sup>76</sup> optimizer with a learning rate of 0.1,  $\beta_1 = 0.5$

and  $\beta_2 = 0.999$  to modify latent vectors. We perform hyperparameter optimization to choose the optimization horizon, described in the SI.

#### 4.5 Structural Refinement

Structural refinement, in the form of local coordinate optimization, proceeds similarly to latent vector optimization. The scoring module is used to repeatedly evaluate ligands, and the derivatives concerning the ligand’s coordinates are used to modify the ligand’s coordinates with a gradient-based optimizer. We use the L-BFGS optimizer in Pytorch<sup>32</sup> to perform coordinate optimization. Our optimization algorithm is implemented with Pytorch and is parallelizable on a GPU. In this work, we only use one combination of evaluators to perform coordinate optimization: torchvina and ANI2x. We discuss the selection of different inter and intramolecular forces in the SI.

## 5 Data Availability

We used the following publicly available datasets for validation and testing: CrossDocked2020 (<https://bits.csb.pitt.edu/files/crossdock2020/>), and Binding MOAD (<http://www.bindingmoad.org/>). Detailed testing splits for generating each of the test benchmarks used in this work are described in <https://github.com/pengxingang/Pocket2Mol/tree/main/data>. A subset of CrossDocked2020 was used to select hyperparameters as described in the SI, and is available at <https://github.com/matragoza/LiGAN/tree/master/data/crossdock2020>. The torchvina and torchSA scoring modules are available at <https://github.com/sandbox-quantum/idolpro-scoring>.

## 6 Acknowledgements

The authors thank Andrea Bortolato, Andrew Wildman, Arman Zaribafiyani, Benjamin Shields, and Jordan Crivelli-Decker for their feedback on the manuscript.

## 7 Author Contributions

AK, KR, and TY conceived the study, designed IDOLpro, and planned the experiments. AK and KR implemented IDOLpro, ran experiments, and wrote the manuscript. EL implemented the lead optimization capability in IDOLpro and wrote the corresponding section in the manuscript. AR and TY advised and reviewed the manuscript.

## References

- 1 A. C. Anderson, *Chemistry & biology*, 2003, **10**, 787–797.
- 2 A. Zunger, *Nature Reviews Chemistry*, 2018, **2**, 0121.
- 3 K. Ryczko, P. Darancet and I. Tamblin, *The Journal of Physical Chemistry C*, 2020, **124**, 26117–26123.
- 4 F. R. J. Cornet, B. Benediktsson, B. A. Hastrup, A. Bhowmik and M. N. Schmidt, 37th Conference on Neural Information Processing Systems, 2023.
- 5 B. Sanchez-Lengeling, C. Outeiral, G. L. Guimaraes and A. Aspuru-Guzik, *ChemRxiv*, 2017.
- 6 N. W. Gebauer, M. Gastegger, S. S. Hessmann, K.-R. Müller and K. T. Schütt, *Nature communications*, 2022, **13**, 973.
- 7 B. Sridharan, M. Goel and U. D. Priyakumar, *Chemical Communications*, 2022, **58**, 5316–5331.
- 8 S. Lee, J. Jo and S. J. Hwang, Proceedings of the 40th International Conference on Machine Learning, 2023, pp. 18872–18892.
- 9 S. Zaman, D. Akhilarov, M. Araya-Polo and K. Chiu, *arXiv preprint arXiv:2311.06297*, 2023.
- 10 T. Weiss, E. Mayo Yanes, S. Chakraborty, L. Cosmo, A. M. Bronstein and R. Gershoni-Poranne, *Nature Computational Science*, 2023, **3**, 873–882.
- 11 J. J. Irwin and B. K. Shoichet, *Journal of Chemical Information and Modeling*, 2005, **45**, 177–182.
- 12 A. Shivanyuk, S. Ryabukhin, A. Tolmachev, A. Bogolyubsky, D. Mykytenko, A. Chupryna, W. Heilman and A. Kostyuk, *Chemistry today*, 2007, **25**, 58–59.
- 13 L. Ruddigkeit, R. Van Deursen, L. C. Blum and J.-L. Reymond, *Journal of Chemical Information and Modeling*, 2012, **52**, 2864–2875.
- 14 P. G. Polishchuk, T. I. Madzhidov and A. Varnek, *Journal of computer-aided molecular design*, 2013, **27**, 675–679.
- 15 S. Luo, J. Guan, J. Ma and J. Peng, *Advances in Neural Information Processing Systems*, 2021, **34**, 6229–6239.
- 16 X. Peng, S. Luo, J. Guan, Q. Xie, J. Peng and J. Ma, Proceedings of the 39th International Conference on Machine Learning, 2022, pp. 17644–17655.
- 17 M. Liu, Y. Luo, K. Uchino, K. Maruhashi and S. Ji, Proceedings of the 39th International Conference on Machine Learning, 2022, pp. 13912–13924.
- 18 J. Guan, W. W. Qian, X. Peng, Y. Su, J. Peng and J. Ma, International Conference on Learning Representations, 2023.
- 19 A. Schneuing, Y. Du, C. Harris, A. Jamasb, I. Igashov, W. Du, T. Blundell, P. Lió, C. Gomes, M. Welling *et al.*, International Conference on Learning Representations, 2023.
- 20 Y. Li, J. Pei and L. Lai, *Chemical science*, 2021, **12**, 13664–13675.
- 21 A. Lugmayr, M. Danelljan, A. Romero, F. Yu, R. Timofte and L. Van Gool, Proceedings of the IEEE/CVF Conference on Computer Vision and Pattern Recognition, 2022, pp. 11461–11471.
- 22 O. Trott and A. J. Olson, *Journal of computational chemistry*, 2010, **31**, 455–461.
- 23 M. Buttenschoen, G. M. Morris and C. M. Deane, *Chemical Science*, 2024, **15**, 3130–3139.

- 24 Y. Yu, S. Lu, Z. Gao, H. Zheng and G. Ke, *arXiv preprint arXiv:2302.07134*, 2023.
- 25 W. Gao and C. W. Coley, *Journal of chemical information and modeling*, 2020, **60**, 5714–5723.
- 26 R. Gómez-Bombarelli, J. N. Wei, D. Duvenaud, J. M. Hernández-Lobato, B. Sánchez-Lengeling, D. Sheberla, J. Aguilera-Iparraguirre, T. D. Hirzel, R. P. Adams and A. Aspuru-Guzik, *ACS central science*, 2018, **4**, 268–276.
- 27 O. Dollar, N. Joshi, J. Pfandner and D. A. Beck, *The Journal of Physical Chemistry A*, 2023, **127**, 7844–7852.
- 28 J. C. Duchi, M. I. Jordan, M. J. Wainwright and A. Wibisono, *IEEE Transactions on Information Theory*, 2015, **61**, 2788–2806.
- 29 G. Corso, H. Stärk, B. Jing, R. Barzilay and T. Jaakkola, International Conference on Learning Representations, 2023.
- 30 C. Devereux, J. S. Smith, K. K. Huddleston, K. Barros, R. Zubatyuk, O. Isayev and A. E. Roitberg, *Journal of Chemical Theory and Computation*, 2020, **16**, 4192–4202.
- 31 *RDKit: Open-source cheminformatics.*, <https://www.rdkit.org>.
- 32 A. Paszke, S. Gross, F. Massa, A. Lerer, J. Bradbury, G. Chanan, T. Killeen, Z. Lin, N. Gimelshein, L. Antiga et al., *Advances in neural information processing systems*, 2019, **32**, 8026 – 8037.
- 33 P. Ertl and A. Schuffenhauer, *Journal of cheminformatics*, 2009, **1**, 1–11.
- 34 P. G. Francoeur, T. Masuda, J. Sunseri, A. Jia, R. B. Iovanisci, I. Snyder and D. R. Koes, *Journal of chemical information and modeling*, 2020, **60**, 4200–4215.
- 35 L. Hu, M. L. Benson, R. D. Smith, M. G. Lerner and H. A. Carlson, *Proteins: Structure, Function, and Bioinformatics*, 2005, **60**, 333–340.
- 36 T. Fu, W. Gao, C. Coley and J. Sun, *Advances in Neural Information Processing Systems*, 2022, **35**, 12325–12338.
- 37 D. R. Koes, M. P. Baumgartner and C. J. Camacho, *Journal of chemical information and modeling*, 2013, **53**, 1893–1904.
- 38 M. M. Mysinger, M. Carchia, J. J. Irwin and B. K. Shoichet, *Journal of medicinal chemistry*, 2012, **55**, 6582–6594.
- 39 C.-H. Zhang, E. A. Stone, M. Deshmukh, J. A. Ippolito, M. M. Ghahremanpour, J. Tirado-Rives, K. A. Spasov, S. Zhang, Y. Takeo, S. N. Kudalkar et al., *ACS central science*, 2021, **7**, 467–475.
- 40 A. Thakkar, V. Chadimová, E. J. Bjerrum, O. Engkvist and J.-L. Reymond, *Chemical Science*, 2021, **12**, 3339–3349.
- 41 J. Yu, J. Wang, H. Zhao, J. Gao, Y. Kang, D. Cao, Z. Wang and T. Hou, *Journal of chemical information and modeling*, 2022, **62**, 2973–2986.
- 42 Schrödinger, LLC.
- 43 M. F. Adasme, K. L. Linnemann, S. N. Bolz, F. Kaiser, S. Salentin, V. J. Haupt and M. Schroeder, *Nucleic acids research*, 2021, **49**, W530–W534.
- 44 G. R. Bickerton, G. V. Paolini, J. Besnard, S. Muresan and A. L. Hopkins, *Nature chemistry*, 2012, **4**, 90–98.
- 45 A. Alhossary, S. D. Handoko, Y. Mu and C.-K. Kwoh, *Bioinformatics*, 2015, **31**, 2214–2216.
- 46 Y. Xie, C. Shi, H. Zhou, Y. Yang, W. Zhang, Y. Yu and L. Li, International Conference on Learning Representations, 2021.
- 47 Z. Zhou, S. Kearnes, L. Li, R. N. Zare and P. Riley, *Scientific reports*, 2019, **9**, 10752.
- 48 S. Ahn, J. Kim, H. Lee and J. Shin, *Advances in neural information processing systems*, 2020, **33**, 12008–12021.
- 49 M. Olivecrona, T. Blaschke, O. Engkvist and H. Chen, *Journal of cheminformatics*, 2017, **9**, 1–14.
- 50 W. Jin, R. Barzilay and T. Jaakkola, International conference on machine learning, 2020, pp. 4849–4859.
- 51 A. Nigam, P. Friederich, M. Krenn and A. Aspuru-Guzik, International Conference on Learning Representations, 2020.
- 52 J. Jensen, *A graph-based genetic algorithm and generative model/Monte Carlo tree search for the exploration of chemical space. Chem Sci 10 (12): 3567–3572*, 2019.
- 53 J. O. Spiegel and J. D. Durrant, *Journal of cheminformatics*, 2020, **12**, 1–16.
- 54 G. Xu, M. C. Abad, P. J. Connolly, M. P. Neeper, G. T. Struble, B. A. Springer, S. L. Emanuel, N. Pandey, R. H. Gruninger, M. Adams et al., *Bioorganic & medicinal chemistry letters*, 2008, **18**, 4615–4619.
- 55 J. P. Hughes, S. Rees, S. B. Kalindjian and K. L. Philpott, *British journal of pharmacology*, 2011, **162**, 1239–1249.
- 56 H.-J. Böhm, A. Flohr and M. Stahl, *Drug discovery today: Technologies*, 2004, **1**, 217–224.
- 57 G. W. Bemis and M. A. Murcko, *Journal of medicinal chemistry*, 1996, **39**, 2887–2893.
- 58 J. E. Crivelli-Decker, Z. Beckwith, G. Tom, L. Le, S. Khuttan, R. Salomon-Ferrer, J. Beall, R. Gómez-Bombarelli and A. Borcolato, *Journal of Chemical Theory and Computation*, 2024, **20**, 7188–7198.
- 59 J. Ho, A. Jain and P. Abbeel, *Advances in neural information processing systems*, 2020, **33**, 6840–6851.
- 60 E. Hoogeboom, V. G. Satorras, C. Vignac and M. Welling, International conference on machine learning, 2022, pp. 8867–8887.

- 61 F. Fuchs, D. Worrall, V. Fischer and M. Welling, *Advances in neural information processing systems*, 2020, **33**, 1970–1981.
- 62 V. G. Satorras, E. Hoogeboom and M. Welling, Proceedings of the 38th International Conference on Machine Learning conference on machine learning, 2021, pp. 9323–9332.
- 63 Y. Song, J. Sohl-Dickstein, D. P. Kingma, A. Kumar, S. Ermon and B. Poole, International Conference on Learning Representations, 2021.
- 64 A. Schneuing, *DiffSBDD*, 2023, <https://github.com/arneschneuing/DiffSBDD>.
- 65 A. H. Larsen, J. J. Mortensen, J. Blomqvist, I. E. Castelli, R. Christensen, M. Dułak, J. Friis, M. N. Groves, B. Hammer, C. Hargus *et al.*, *Journal of Physics: Condensed Matter*, 2017, **29**, 273002.
- 66 S. P. Ong, W. D. Richards, A. Jain, G. Hautier, M. Kocher, S. Cholia, D. Gunter, V. L. Chevrier, K. A. Persson and G. Ceder, *Computational Materials Science*, 2013, **68**, 314–319.
- 67 Z. Wang, L. Zheng, S. Wang, M. Lin, Z. Wang, A. W.-K. Kong, Y. Mu, Y. Wei and W. Li, *Briefings in Bioinformatics*, 2023, **24**, bbac520.
- 68 A. T. McNutt, P. Francoeur, R. Aggarwal, T. Masuda, R. Meli, M. Ragoza, J. Sunseri and D. R. Koes, *Journal of cheminformatics*, 2021, **13**, 1–20.
- 69 R. Quiroga and M. A. Villarreal, *PloS one*, 2016, **11**, e0155183.
- 70 G. Skoraczyński, M. Kitlas, B. Miasojedow and A. Gambin, *Journal of Cheminformatics*, 2023, **15**, 6.
- 71 X. Gao, F. Ramezanghorbani, O. Isayev, J. S. Smith and A. E. Roitberg, *Journal of chemical information and modeling*, 2020, **60**, 3408–3415.
- 72 J. S. Smith, O. Isayev and A. E. Roitberg, *Chemical science*, 2017, **8**, 3192–3203.
- 73 J. S. Smith, B. Nebgen, N. Lubbers, O. Isayev and A. E. Roitberg, *The Journal of chemical physics*, 2018, **148**, 241733.
- 74 J. S. Smith, B. T. Nebgen, R. Zubatyuk, N. Lubbers, C. Devereux, K. Barros, S. Tretiak, O. Isayev and A. E. Roitberg, *Nature communications*, 2019, **10**, 2903.
- 75 D. Folmsbee and G. Hutchison, *International Journal of Quantum Chemistry*, 2021, **121**, e26381.
- 76 D. P. Kingma and J. Ba, International Conference on Learning Representations, 2015.

## S Supplementary Information

### S.1 More details of the SA model

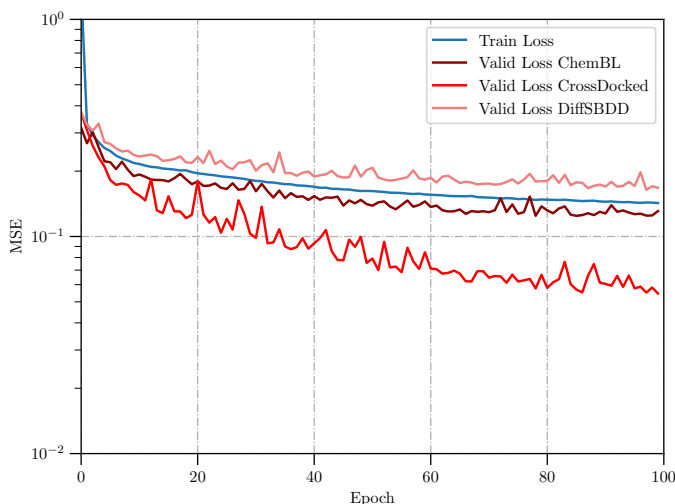


Fig. S1 Training and validation curves for training PaiNN to predict the SA score on 3D atomic point clouds. The MSE at each epoch is plotted for the training set, the ChemBL validation set, the DiffSBDD validation set, and the CrossDocked validation set.

To train the SA model, we prepare a dataset consisting of all molecules with structural information in ChemBL<sup>77</sup> (2,409,270 structures), and ligands used to train DiffSBDD<sup>19</sup> on CrossDocked2020<sup>34</sup> (183,468 structures). Although the SA score is fully determined by the chemical graph of a molecule, we keep molecules with different conformations from CrossDocked2020 to aid the model in learning the redundancy of pose in determining the SA score. To improve the model’s performance on ligands produced by DiffSBDD, we generate nearly 1,000,000 (877,284) ligands with DiffSBDD which are included in the training data. We generate several ligands for each of the protein pockets in the DiffSBDD training set and then filter them using the same validity checks described in the Methods section. We put a higher emphasis on modelling ligands from CrossDocked2020 and DiffSBDD, sampling from one of these datasets during training with a  $5\times$  higher likelihood than ChEMBL.

We train the polarizable atomic interaction neural network<sup>78</sup> (PaiNN) from the Open Catalyst Project<sup>79,80</sup> to predict the SA score given the atomic coordinates and atom types. To allow PaiNN to make predictions on atom types coming out of DiffSBDD, we encode atom types as one-hot vectors. We first optimize the hyperparameters of the model using Ray Tune<sup>81</sup>. The hyperparameters chosen were  $num\_rbf = 64$ ,  $num\_layers = 4$ ,  $max\_neighbor = 30$ ,  $cutoff = 8.0$ ,  $hidden\_channels = 256$ . We use a 95%/5% training/validation split for each dataset. The model is trained for 100 epochs to minimize the MSE loss with the AdamW optimizer<sup>82</sup> with a learning rate of  $5 \times 10^{-4}$ . Training and validation curves are plotted in Fig. S1.

### S.2 Hyperparameter Tuning

We perform several hyperparameter tuning experiments to fine-tune the performance of our pipeline. To avoid overfitting on

our two benchmark sets, we perform all experiments using a non-overlapping validation set. This validation set is composed of 10 targets taken from the test set of LiGAN<sup>83</sup>, which was used to validate the performance of several other works in the literature<sup>17,84</sup>. For each of these ten targets, a single pocket is randomly selected to be included in the validation set. The set of receptor-ligand combinations used in these experiments is included in Table S1. We generate 20 ligands per pocket for each experiment. Each experiment is run on an NVIDIA A10G GPU with 24 GB of GPU memory.

#### S.2.1 Accelerating Diffusion

In DiffSBDD, the models are trained to generate ligands over 500 reverse diffusion steps according to some noise schedule. At each time step an equivariant network takes in the noised coordinates and atom types, as well as the time step, and returns a denoised representation of the atoms and coordinates<sup>19</sup>. One can reduce the number of reverse diffusion steps by skipping time steps in the noise schedule.

In IDOLpro, the majority of the reverse diffusion process is run to generate  $\mathbf{z}_{t_{hz}}$ , i.e., to seed the initial latent vectors. When optimizing  $\mathbf{z}_{t_{hz}}$ , the rollout of  $\mathbf{z}_{t_{hz}}, \dots, \mathbf{z}_0$  needs to be repeated many times. We run an experiment to determine whether we can reduce the number of steps during this final rollout 10-fold without a significant degradation in performance. We run an experiment with the smallest horizon considered  $t_{hz} = 50$ . Results are shown in table Table S2. Running the rollout with reduced diffusion steps results in over a  $3\times$  speedup, with a slight decrease in average Vina score ( $< 0.5$  kcal/mol), while preserving average SA and QED. We adopt this setting in our pipeline for this reason.

#### S.2.2 Tuning Optimization Horizon

We tune the value of the optimization horizon,  $t_{hz}$ , to optimize both the Vina and SA scores of generated molecules. We consider  $t_{hz} \in 50, 100, 200$ . For each setting of the optimization horizon, we track the difference in Vina score, SA score, and QED. Results are reported in Table S3. Based on these results we set the optimization horizon to 200, since that setting resulted in by far the best difference in Vina score and QED, albeit a slightly worse improvement in SA score relative to setting  $t_{hz} = 100$ .

#### S.2.3 Structural Refinement with Torchvina and ANI2x

Here we discuss how we tune the performance of our structural refinement procedure. We consider various combinations of intra-molecular and inter-molecular forces derived from the torchvina and ANI2x<sup>30</sup> potentials. We use the following parameters in the L-BFGS optimization algorithm:  $max\_iter=100$ ,  $tolerance\_grad=10^{-3}$ , and  $line\_search\_fn="strong\_wolfe"$ . For each experiment, we keep track of the average Vina score, the top-10% Vina score, the average time taken to optimize each ligand, and the percent of valid structures that are output by the procedure based on our validity checks. We tabulate these results in Table S4 and include the same metrics when QuickVina2<sup>45</sup> is used for docking for comparison. QuickVina2 was used to dock structures after generation in DiffSBDD<sup>19</sup>.

When analyzing the reason for invalid molecules, we find that a large number of failed cases are due to atoms becoming too far

PDB ID	Ligand ID
2ah9	cto
5lvq	p2l
5g3n	u8d
1u0f	g6p
4bnw	fxe
4i91	cpz
2ati	ihu
2hw1	lj9
1bvr	geq
1zyu	k2q

Table S1 Validation set used to choose hyper-parameters in IDOLpro. All proteins from the test set of LiGAN<sup>83</sup> were used, and a single protein pocket for each protein was selected at random.

Diffusion steps	Vina [kcal/mol]	SA	QED	Time [s]
5	$-6.25 \pm 2.08$	$3.72 \pm 0.46$	$0.53 \pm 0.10$	$60.60 \pm 49.75$
50	$-6.72 \pm 2.45$	$3.92 \pm 0.58$	$0.54 \pm 0.10$	$196.96 \pm 102.97$

Table S2 Results when reducing the number of rollout steps from 50 to 5. The average Vina, SA, and QED across the validation set is reported.

$t_{hz}$	$\Delta$ Vina	$\Delta$ SA	$\Delta$ QED
50	-1.21	-0.34	-0.028
100	-1.17	-0.82	0.004
200	-1.84	-0.76	0.048

Table S3 Results when varying the optimization horizon  $t_{hz}$  in IDOLpro. The difference in Vina, SA, and QED for the final optimized ligands produced by IDOLpro relative to the initial ligands produced by DiffSBDD are reported.

Method	Torchvina	ANI2x	L1 bond penalty	Vina [kcal/mol]	Vina <sub>10%</sub> [kcal/mol]	Validity [%]	Time [s]
QuickVina2	-	-	-	-8.51	-9.51	95.0	75.0
IDOLpro	Inter+Intra	Inter+Intra	$\times$	-9.26	-10.35	80.1	19.34
IDOLpro	Inter+Intra	Intra	$\times$	-9.33	-10.41	77.2	22.49
IDOLpro	Inter	Inter+Intra	$\times$	-9.38	-10.53	82.1	18.53
IDOLpro	Inter	Intra	$\times$	-9.53	-10.70	81.6	23.90
IDOLpro	Inter	Intra	$\checkmark$	-9.39	-10.68	86.6	24.45

Table S4 Results when running structural refinement various combinations of inter-molecular and intra-molecular forces derived from the Vina and ANI2x potentials. We also make note of whether an L1 penalty for enforcing bonds was used. For each experiment, we note the Vina score, top-10 Vina score. We also make note of the percent of valid structures produced with the combination of potentials. Lastly, we report the minimum amount of valid structures produced on a single test case. Validity checks are performed according to the checks described in Section Validity Checks.

during the structural relaxation, causing the molecule to become disconnected. To remedy this, we add an L1 penalty for violating the bonds in the molecule produced by IDOLpro. To do so, we use ASE’s<sup>65</sup> natural cutoffs. We find that setting a weight of 0.01 on this L1 penalty result in the best balance of Vina score and validity.

#### S.2.4 Stopping Criteria, Backtracking, and Decaying Learning Rate

We use per-parameter options in Pytorch<sup>32</sup> to allow for individualized learning rates for different ligands. For each ligand, we optimize it with Adam with the chosen hyperparameters. We optimize each latent vector for 10-200 optimization steps. Often, during latent vector optimization, a ligand will be pushed to a part of latent space such that it becomes invalid. In such a case, we attempt to generate a ligand 10 times with the given latent vector. If after 10 attempts, reverse diffusion has not produced a valid ligand, we backtrack to the previous latent vector in the optimization trajectory, reduce the learning rate by a factor of 10, and restart the optimization. If at another point in the optimization, with the reduced

learning rate, another latent vector fails to generate a valid ligand over 10 attempts, the optimization of that trajectory is stopped.

#### S.3 An Additional Scoring Function: DiffDock

We include the scoring module from DiffDock<sup>29</sup> in our evaluator module. DiffDock is composed of two modules, a docking module and a scoring module, which together can dock ligands to a target protein without pocket information. The DiffDock docking module was trained to predict the experimental binding pose of ligands in the PDBBind dataset<sup>85</sup>. The DiffDock scoring module was trained on experimental data where the goal of the model was to classify whether or not a candidate ligand is  $< 2 \text{ \AA}$  of the experimental binding pose. DiffDock docks ligands by producing many binding poses for a target ligand with the docking module, and returning these poses as a ranked list using the scoring module. The node from the final classification layer of the scoring network, indicating the likelihood that a docked ligand is  $< 2 \text{ \AA}$  from an experimentally derived binding pose, can be used as a scoring function.

DiffDock was shown to have state-of-the-art performance on a blind docking task for protein-ligand pairs extracted from the PDB-Bind dataset, significantly outperforming other state-of-the-art ML-based docking procedures<sup>29</sup>.

#### S.4 Visualization of Latent Vectors

Latent vector visualization was performed with UMAP<sup>86</sup> and visualized in Fig. S2.

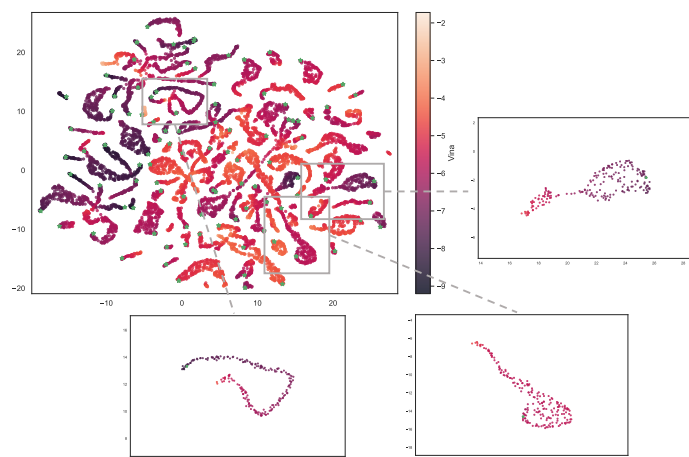


Fig. S2 Latent vector visualizations of IDOLpro when generating ligands for 14gs. The points are coloured by Vina score (darker implies lower scores), and a green star marks the end of each optimization trajectory.

#### Supplementary References

- 77 B. Zdrzil, E. Felix, F. Hunter, E. J. Manners, J. Blackshaw, S. Corbett, M. de Veij, H. Ioannidis, D. M. Lopez, J. F. Mosquera *et al.*, *Nucleic acids research*, 2024, **52**, D1180–D1192.
- 78 K. Schütt, O. Unke and M. Gastegger, *International Conference on Machine Learning*, 2021, pp. 9377–9388.
- 79 L. Chanussot, A. Das, S. Goyal, T. Lavril, M. Shuaibi, M. Riviere, K. Tran, J. Heras-Domingo, C. Ho, W. Hu *et al.*, *Acs Catalysis*, 2021, **11**, 6059–6072.
- 80 R. Tran, J. Lan, M. Shuaibi, B. M. Wood, S. Goyal, A. Das, J. Heras-Domingo, A. Kolluru, A. Rizvi, N. Shoghi *et al.*, *ACS Catalysis*, 2023, **13**, 3066–3084.
- 81 R. Liaw, E. Liang, R. Nishihara, P. Moritz, J. E. Gonzalez and I. Stoica, *arXiv preprint arXiv:1807.05118*, 2018.
- 82 I. Loshchilov and F. Hutter, *International Conference on Learning Representations*, 2019.
- 83 M. Ragoza, T. Masuda and D. R. Koes, *Chemical science*, 2022, **13**, 2701–2713.
- 84 H. Lin, Y. Huang, M. Liu, X. Li, S. Ji and S. Z. Li, *arXiv preprint arXiv:2211.11214*, 2022.
- 85 R. Wang, X. Fang, Y. Lu, C.-Y. Yang and S. Wang, *Journal of medicinal chemistry*, 2005, **48**, 4111–4119.
- 86 L. McInnes, J. Healy and J. Melville, *arXiv preprint arXiv:1802.03426*, 2018.